Analysis of SIV Spatiotemporal Dissemination Patterns in Rhesus Macaques During Early Rectal Transmission Demonstrates Systemic Infection Does Not Require Viral Local Amplification at the Entry Portal

Yilun Cheng[1], Jackson Chen,[1,2], Miaoyun Zhao[1,2], Subhra Mandal[1], Mark G Lewis[3], Ma Luo[4,5], Michael Gale, Jr.[6,7] Qingsheng Li[1,2*]

[1]Nebraska Center for Virology and School of Biological Sciences, University of Nebraska-Lincoln, Lincoln, NE, USA.

[2] The Wistar Institute, HIV-1 Cure and Viral Diseases Center, 3601 Spruce Street Philadelphia, PA, USA.

[3] BIOQUAL, Inc., Rockville, MD, USA.

[4]Department of Medical Microbiology and Infectious Diseases, University of Manitoba, Winnipeg, Manitoba, Canada. [5]National Microbiology Laboratory, Public Health Agency of Canada, Winnipeg, Manitoba, Canada.

[6]Department Department of Microbiology and Immunology, University of Minnesota, [7]Institute on Infectious Diseases, University of Minnesota, MN, USA.

* Corresponding author:

Qingsheng Li, qli@wistar.org

Abstract:

Receptive anal sex is a dominant mode of HIV-1 (HIV) transmission, especially among men who have sex with men (MSM). However, the early events during HIV rectal transmission are not well understood and many questions remain, such as, does virus local amplification at the entry portal require for viral distal seeding? What is the spatiotemporal dissemination pattern across whole body? How do three viral forms, e.g., cell-free virus (V_{CF}), cell-associated virus (V_{CA}), and follicular dendritic cell-trapped virus (V_{FDC}), evolve during early infections? To close this knowledge gap, we comprehensively examined rectum, draining and distant lymph nodes, as well as non-lymphatic organs of brain, lungs, and liver of 39 Indian rhesus macaques at the early time points following intrarectal SIV inoculation (1, 2, 3, 4, 6, 10 14, 28 day post inoculation, dpi). Our findings unambiguously demonstrated SIV rapidly disseminates to distant tissues and organs (<=1 dpi), virus local replication and amplification in rectum and draining lymph nodes are not required for viral distal seeding for the establishment of systemic infection, viral forms shift from V_{CF} and V_{CA} to V_{FDC} accompanying from T-cell zones into B-cell follicles. These findings indicates that an effective HIV vaccine needs to elicit comprehensive immune protection locally at sites of viral entry as well as systemically.

Keyword: HIV/SIV early rectal transmission, local viral amplification, systemic infection, HIV vaccine

INTRODUCTION

Viral infection often begins with viruses crossing the mucosal barrier and disseminating to distal sites through blood circulation, lymphatic system, neurological pathways along or in combination. A better understand of virus dissemination patterns and the role of virus local amplification at the portal of entry after exposure is critical for developing vaccines and pre- and post-exposure prophylaxis. Different viruses have distinct dissemination patterns after the exposure. For example, rabies virus dissemination follows a multi-stage process where viral local replication and amplification in muscle tissues after animal bite and scratch is critical for virus dissemination and widespread infection in the central nervous system (1, 2) and Poliovirus local replication and amplification in the pharynx and the gastrointestinal tract has been demonstrated to be required for spreading to the central nervous system (3). However, the role of HIV local replication and amplification at the portal of entry for systemic infection is unknown.

HIV infection remains a global health threat. About 39 million people are living with HIV worldwide. Despite the presence of a combined antiretroviral therapy (ART) and several preventive measures, approximately 1.3 million new HIV infections were still reported in 2022 (https://unaids.org/en). Receptive anal sex is a major mode of HIV transmission, especially in men who have sex with men (MSM) (4-7), which accounted for 66% of all new HIV diagnoses in males in the United States (CDC, HIV surveillance report 2024, https://www.cdc.gov/hiv-data/nhss/hiv-diagnoses-deaths-and-prevalence-2025.html). Moreover, HIV vaccine development over the past 4 decades has made some progress, however, vaccines that prevent infection remain elusive. Thus, a better understanding of very early events of HIV mucosal transmission and viral spatiotemporal distribution patterns crossing whole body, including viral entry site, draining and distal lymphatic organs and non-lymphatic organs, especially the role of viral local amplification at the portal of entry in the establishment of systemic infection, is needed for guiding HIV vaccine development (7-11).

For the relative ease of procurement and ready availability of peripheral blood in clinical research, most investigations on HIV transmission have primarily depended on the continuous monitoring of peripheral blood samples (12-14). However, HIV target cells are mainly localized in mucosal and the secondary lymphatic tissues (LTs) and there is an eclipse phase between the point of initial infection to the time of viremia (15, 16). Due to ethical constraints in humans, in vivo data regarding viral entry and early dissemination patterns can only be studied using rhesus macaques (RMs) Simian Immunodeficiency virus (SIV) models (17, 18). Nevertheless, previously published RM SIV rectal transmission studies mainly focused on infection at the entry site and viral-host mucosal interactions (19-21). Patricia and colleagues found that SIV viral DNA was detected as early as 4 hours pi in colic lymph nodes, but not in axillary lymph nodes (LNs) until 2 dpi (5), Sui and colleagues reported only 15% RMs had detectable viral RNA (vRNA) in the plasma as early as 4 day pi (6). Mair and colleagues reported that at 48 hours pi, infected cell foci consisting of only a few cells scattered throughout the anal and rectal tissues. (22). We previously reported that SIV vRNA was only detectable in the rectum at 3 dpi but not 1 and 2 dpi using S^{35} labeled SIV riboprobe in situ hybridization (ISH), which was much less sensitive than RNAscope ISH(19). In short, there was a significant knowledge gap in the very early events of HIV rectal transmission before the current study.

In this research, we comprehensively evaluated the viral spatiotemporal distribution patterns across whole body, the dynamic change of viral forms, and the role of virus local amplification for the establishment of systemic infection using a highly sensitive RNAscope ISH (RNAscope) and a combination of CODEX (CO-Detection by inDEXing) immunostaining with RNAscope ISH (Comb-CODEX-RNAscope). We found that virus local amplification at the portal of entry and draining lymph nodes (dLN) are not required for viral systemic infection; at 1 dpi, vRNA were readily detected not only in the rectal and its dLN, but also in the distal LN (disLN) as well as non-lymphatic organs of liver, lungs and brain. These findings support a new model of HIV rectal

transmission where HIV rapidly seeds to distal sites and viral local amplification is not required for the establishment of systemic infection. These findings suggest that an effective HIV vaccine needs to elicit robust immune protections at both the portal of viral entry and at the systemic level.

MATERIALS AND METHODS

Animals and Ethics Statement

This report studied the samples from two cohorts of adult male rhesus macaques (*Macaca mulatta*) of Indian origin. All the animals were specific pathogen free (SPF, negative for HIV-2, SIV, type D retrovirus, and simian type D retrovirus 1) and without the protective major histocompatibility complex class I alleles of Mamu A01, B01, and B17. The first macaque cohort study was approved by the Institutional Animal Care and Use Committee at the University of Nebraska-Lincoln and BIOQUAL, Inc. The rhesus macaque animal work was conducted at BIOQUAL, Inc. (Rockville, Maryland). Twenty macaques were intrarectally inoculated with SIVmac251 at a dose of 3.1 x 10^4 TCID50 and were euthanized at various time points of post inoculation (3 animals at each time points of 3, 10, 14 and 28 dpi and 4 animals at 4 and 6 dpi), while three rhesus macaques without virus challenge were served as uninfected controls (n=3). The second cohort macaque study was approved by the University of Washington Environmental Health and Safety Committee, the Occupational Health Administration, the Primate Center Research Review Committee, and the Institutional Animal Care and Use Committee. The rhesus macaque animal work was conducted at the Washington National Primate Research Center. The macaques were intrarectally inoculated with SIVmac251 at a dose of 6000 $TCID_{50}$ and were euthanized at various time points (n=4 at 1, 2, 3, 4 dpi). All the tissues during necropsy were fixed with SafeFix II (Cat# 23-042600, Fisher Scientific), 4% paraformaldehyde or neutral-buffered formalin and embedded with paraffin as we previously reported (20, 23).

RNAscope In Situ Hybridization (RNAscope)

RNAscope was performed according to our previously published method(24, 25). RNAscope® Probe-SIVmac239 (anti-sense, Cat# 312811, Advanced Cell Diagnostics, ACD) was used and the signals were amplified and detected with RNAscope® 2.5 HD assay-Red kit (Cat# 322360, ACD). The RNAscope® negative control probe-DapB (Cat# 310043, ACD) was used as negative probe control and uninfected macaque tissues were used as negative tissue control. Tissue sections on slides after RNAscope were digitized using the Aperio ScanScope into an image server and perform image quantification analysis using our Aperio Spectrum system as we previously reported (25).

Antibody-oligonucleotide conjugation:

To conjugate a rhesus macaque reactive CD3 antibody for CODEX, an anti-human CD3 antibody in a carrier-free PBS solution (Clone#: SP162, Cat#: ab245731, Abcam) was conjugated with the barcode-oligonucleotide (Cat#: 5350002, Akoya) using CODEX conjugation kit (Cat#: 7000009, Akoya) following CODEX conjugation manual as we previously reported(26).

Combination of CODEX immunostaining with RNAscope ISH (Comb- CODEX- RNAscope)

CODEX (Co-detection by indexing) is a cutting-edge multiplexed tissue imaging technology that enables simultaneous visualization of dozens of protein markers while preserving tissue architecture. Comb-CODEX-RNAscope enables detection of viral RNA via RNAscope and dozens of proteins via CODEX concurrently. The Comb-CODEX-RNAscope was performed according to our previously published method (26). We used the protocol of CODEX first and subsequent RNAscope approach and we combined pretreatments of CODEX and RNAscope together at the beginning of Comb-CODEX-RNAscope (26). Briefly, 6-µm tissue sections were mounted on poly-lysine-coated coverslips. The deparaffinization process began by heating

samples in a 60°C incubator for 2 hours, followed by two 5-minute xylene washes. Samples were then rehydrated through a series of decreasing ethanol concentrations and DEPC water. Prior to initiating the CODEX cycling, tissues section on coverslip was pretreated with 3% hydrogen peroxide and citrate antigen retrieval buffer (Sigma 21545).

The retrieved tissues were then incubated with a DNA-barcoded antibody mixture for 3 hours at room temperature. Unbound antibodies were removed through three consecutive 2-minute PBS washes. Post-fixation occurred in two stages: first with 1.6% paraformaldehyde for 10 minutes at room temperature, followed by washing and a second fixation step using ice-cold methanol for 5 minutes. After additional washing, samples were stored in buffer at 4°C for up to five days or immediately processed in the CODEX instrument. Fluorescent reporters consisting of labeled oligonucleotide probes matching the DNA-barcoded antibodies were prepared in a 96-well plate according to manufacturer specifications. The CODEX fluidics system and Keyence microscope operated under control of the CODEX instrument manager and Keyence software following standard protocols. Upon completion of CODEX cycling, tissue-coverslips were transferred to the RNAscope workflow beginning at the protease plus treatment step. Following RNAscope completion, tissue sections were counterstained with DAPI (1:2000 dilution) for 5 minutes at room temperature, washed, and returned to the CODEX instrument for RNAscope image acquisition. Integration of RNAscope data with CODEX images requires adding a blank cycle with Cy5-channel assignment for RNAscope detection. Final image data was processed using CODEX processor software after transferring to the appropriate file location.

Data Analysis for the Comb-CODEX-RNAscope

After the processing of Comb-CODEX-RNAscope raw data with CODEX processor software, FlowJo v10 with CodexMAV extension was used to analyze data. Flow cytometry like gating strategy was used to determine cell populations based on spatial location and markers. The

statistical analysis and figures of cell populations and viral load dissemination patterns were made with Graphpad Prism 9.5.

Spatial Cluster Analysis of vRNA Distribution

Spatial analysis of vRNA distribution (Figure 4) was performed using QuPath software (https://qupath.github.io/). Prior to analysis, the metadata for all whole tissue section images was manually verified to ensure correct pixel size calibration. A pixel classifier was first trained to segment tissue regions by distinguishing tissue from the white background. To separate the stains, color deconvolution was performed. Initial stain vectors for nuclear stains with Hematoxylin and vRNA signal of Fast Red were identified using the 'Estimate Stain Vectors' command, followed by manual adjustment to ensure optimal stain separation. Following segmentation, vRNA-positive signals were identified using the 'Positive Cell Detection' command. The analysis was run at a requested pixel size of 0.5 µm/pixel. Key parameters were set as follows: the background radius was 5 µm, the minimum and maximum detection areas were set to 0.5 μm^2 and 5.0 μm^2, respectively, and cell expansion was set to 0 µm.

To identify spatial clusters of vRNA-positive cells, the Density-Based Spatial Clustering of Applications with Noise (DBSCAN) algorithm was subsequently applied(27). The algorithm's parameters were set with an epsilon (maximum search radius) of 50 µm and a minimum of 3 points (minPts) required to form a dense cluster.

RESULTS

SIV fast disseminates to draining and distal lymphatic tissues as well as non-lymphatic organs of lungs, liver and brain during very early rectal transmission.

To assess SIV spatiotemporal dissemination after rectal transmission, adult male *Indian* rhesus macaques (RMs) were intrarectally inoculated with a swarm of SIVmac251. The RMs were

euthanized at early time points of 1 (24 hrs)-, 2 (48 hrs)-, 3-, 4-, 6-, 10-, 14-, and 28-days post inoculation (dpi, Fig. 1). Additionally, three RMs without SIV inoculation were euthanized to serve as uninfected controls (Fig 1). A comprehensive necropsy was performed on each animal to collect samples, including rectum, draining lymph nodes (dLN, mesenteric) of rectum, distal lymph nodes (disLN, axillary and mandibular), spleen, and non-lymphatic organs of liver, lung, and brain tissues (Fig.1). Tissue samples were divided into three portions for Safefix II fixation, 4% PFA fixation, and snap-freezing, respectively. Peripheral blood mononuclear cells (PBMC) were isolated before and after virus inoculation, and plasma was stored at -80C for SIV vRNA quantification using qRT-PCR.

To detect SIV viral RNA (vRNA) in tissues that were collected during necropsies as described above, RNAscope using SIVmac239 anti-sense probe (Cat# 312811, ACD) was performed, of which the detection sensitivity is a single copy of vRNA. The RNAscope® negative control probe-DapB (Cat# 310043, ACD) was used as negative control and vRNA signals were negative in the uninfected control RMs by RNAscope with SIVmac239-anti-sense-probe. On 1 dpi (24 hrs pi), vRNA was readily detected in the rectal tissues and mesenteric dLN tissues of all 4 animals (Fig. 2). Importantly, vRNA was also detected in the disLN tissues of axillary and mandibular lymph nodes (Fig. 2) and non-lymphatic organs of lungs, liver and frontal cortex and basal ganglion of brain (Fig. 3, sTable 1), demonstrating that at 1 dpi, SIV already disseminated from the portal of rectal entry to dLN, disLN, non-lymphatic organs of lungs, liver and brain. Of note, the frequency and abundance of detected vRNA signals were extremely low, manifesting as a single dot, which morphologically resembles a single virion derived signal. At 2-, 3- (Fig 4 and sTable 1) and 4-dpi and thereafter, vRNA signals were readily detected in all the tissues and all the animals that we examined, including rectal, dLN, disLN, and non-lymphatic organs of lungs, brain and liver. To our knowledge, this is the first study that comprehensively investigated the

spatiotemporal viral dissemination patterns across tissues and organs in such an early timeframe using the highly sensitive RNAscope.

Virus Local Amplification at the Portal of Entry Is Not Required for the Establishing of Systemic infection.

To determine whether viral distal seeding is the consequence of viral local amplification at the portal of entry and dLN, we ran a spatial cluster program to quantify virus replication and amplification clustering. A viral cluster is defined as 3 or more distinct virions derived from vRNA signals in a closely adjacent area of smaller than 50um in radius. As the diameter of CD4 T cells is generally 5–10 µm depending on the differentiation and activation state (28) and three or more of virion in such as small area indicate viral local amplification. On 1 dpi when vRNA was detected in disLN, spleen and non-lymphatic organs of liver, lungs and brain, we did not find any vial clusters in rectal, dLN, disLN tissues in all four animals (Fig. 2), indicating virus local replication and amplification at portal of rectal entry and dLN is not essential for virus distal seeding. We only detected viral clusters in dLN and disLN tissues on 2, 3, and 4 dpi (Fig.4) and thereafter, when SIV already disseminated to distal tissues and organs, indicating vRNA replication and amplification across the body after establishing the systemic infection. To our knowledge, this is the first study shows the evidence that SIV local amplification at the portal of entry is not required for the establishment of systemic infection.

The Spatiotemporal Distribution Patterns of Three Different Vial Forms and Virally Infected CD4 and Macrophage during Early Rectal Transmission

Three viral forms, e.g. cell-free (V_{CF}), cell-associated (V_{CA}), and follicular dendritic cells (FDC)-trapped (V_{FDC}), coexist in vivo in the secondary lymphatic tissues (LTs) during HIV infection. Different viral forms play distinct roles in the establishment and maintenance of infection and pathogenesis. FDC localizes in the light zones of germinal center in B-cell follicles of the LTs,

which can trap virions for an extremely long-period of time via immune complex. V_{FDC} has been demonstrated to be infectious to migrating CD4 T follicular help cells (Tfh) that play an important role in the HIV pathogenesis(29). In the very early infection (≤6dpi), all the SIV vRNA we detected are V_{CA} and V_{CF} (single dot outside cells) (Fig 5A). V_{FDC} was first detected on 10 dpi and became dominant viral form in LTs at 14 and 28 dpi (Fig.5).

To quantitatively examine the spatial distribution patterns of virally infected CD4 T cells and macrophages in LTs during early rectal infection, we used the Comb-CODEX-RNAscope (26) to visualize and quantify vRNA and multiple immune cell protein markers simultaneously. A cocktail of antibodies to CD3, CD4, CD68, CD20, CD21, CD31, Ki67, HLA-Dr, and IDO were used to identify immune cell types and immune activation state in combination with vRNA detection. Figure 6 (Rh5429, 28dpi) shows representative images for the co-detection of vRNA and various immune markers. Using the Comb-CODEX-RNAscope, we found that CD4 T cells are the primary cell type that supports productive viral replication, making up greater than 90% of all productively infected cells, while infected macrophages constitute a minor fraction below 10%. To examine the spatial distribution patterns of virally infected CD4 T cells and macrophages in LTs during early infection, we quantified v*RNA*+ CD4 T cells and macrophages in T-cell zones and B-cell follicles of LN tissues at 10. 14, 28 dpi (n=3/each). We first identified virally infected CD4 (CD4+ & vRNA+) or macrophage (CD68+ & vRNA+) by combining two channels of signals, then used the B-cell follicle marker of CD20 as a gate to demarcate virally infected cell localizations in B-cell follicles or T- cell zones. We found that the distribution patterns of virally infected CD4 T cells shifted from mainly in T-cell zones at 10 dpi to mainly in B-cell follicles at 14 and 28 dpi (Fig. 7A). This shift is also true for virally infected macrophages (Fig. 7B), which are paralleled with the shift of vRNA loads mainly in T-cell zones at 10 dpi to the B-cell follicles at 14 and 28 dpi in the viral form of V_{FDC} (Fig. 7C).

We also quantified vRNA in T-cell zones and B-cell follicles, CD4 T cell counts and immune activation markers in the LN tissues of macaques of 0, 1, 2, 3, 6, 10 and 28 dpi (n=4 at 1, 2, 3 dpi, n=3 at 0, 6, 10, 14, 28 dpi). SIV vRNA in vivo growth curve in T-cell zones peaked at 10 dpi and then declined (Fig. 7D), while in B-cell follicles were significantly increased at 10 dpi and maintained at a high level till 28 dpi (Fig. 7E). Moreover, there was a significant CD4 T cells decline and a significantly increased expression of immune activation markers of ki67, HLA-Dr (Supplemental Fig. 3) as well as immune suppression protein marker of Indoleamine 2,3-dioxygenase 1 (IDO1) that may counteract the general immune activation induced by SIV infection (Supplemental Fig. 3).

Discussion

The period following initial mucosal exposure to HIV and preceding systemic viral dissemination constitutes a critical window during which interventions could be most effective (30, 31). In this study, we unambiguously demonstrated that SIV rapidly disseminated to rectal, draining lymph nodes (dLN), distal lymph nodes (disLN) and spleen as well as non-lymphatic organs of liver, lungs and brain at 1 day post inoculation (dpi) in all 4 macaques we studied using the ultra-sensitive RNAscope that enables to detect single SIV virion. We detected both V_{CA} and V_{CF} in dLN, disLN and non-lymphatic organs of lung, brain and liver at 1dpi, indicating that both blood and lymphatic circulation are likely involved in this early dissemination process (Fig. 2 and 3). Our findings align with the recent research conducted by Whitney and colleagues (14) that examined the effects of initiating ART at 6 hours and 1 day following intrarectal SIVmac251 infection. Following cessation of the 6-month ART regimen, viral rebound rates were 0% in animals that began treatment at 6 hours post-infection and 20% in those that started treatment at 1 dpi. Historically using less sensitive viral detection methods, it was believed that a prolonged local viral amplification phase for small founder populations of infected cells near the

portal of entry is essential for the establishment of systemic infection (10, 32-37). Deleage, C and colleagues, using barcoded-virus experiments and high-resolution mapping, indicate that multiple microfoci within the female genital tract appear very early (hours–days) preceded lymphatic dissemination, also before expansion and spread to distal sites (35). In the past, tissue-level studies using radiolabeled ISH and immunohistology showed high LN viral loads early after a few days of infection (24), and more modern RNAscope approaches have significantly increased detection sensitivity and allowed cell-type colocalization (26, 38-40). A convergence of data from rigorous necropsy studies in non-human primate rectal inoculation models now reveals a dramatically accelerated timeline of systemic infection (35, 41-43). However, the whole-body analysis of viral spatiotemporal distribution patterns following early rectal transmission is unknow until this study.

To determine the role of viral local amplification at the portal of rectal entry and dLN for distal seeding and the establishment of systemic infection, we comprehensively analyzed vRNA spatial distribution patterns in rectal, dLN and disLN in macaques on 1, 2, 3, 4 dpi. We hypothesized that if a local viral amplification plays a crucial role for distant viral seeding during initial systemic dissemination (1 dpi), then the evidence of viral local replication and expansion should be detectable within rectal and dLN tissues. We tested this hypothesis by using ultra-sensitive RNAscope and extensively examining vRNA in multiple sections of rectum, dLN, however we did not detect any viral cluster, which is defined as at least 3 viruses within 50 micron radium (about 5-8 T cell distance), indicating that viral local replication is not essential for virus distal seeding and establishment systemic infection. These findings suggest that an effective HIV vaccine needs to protect not only the portal of viral entry but also at systemic level.

To better understand the spatiotemporal virus distribution patterns and early virus-host interaction, in this study, we employed the Comb-CODEX-RNAscope to visualize and quantify

vRNA and immune cell markers concurrently in LTs and found that productively infected $CD4^+$ T cells dominate early infected-cell populations, while infected macrophages are secondary. Using the Comb-CODEX-RNAscope and spatial analysis, we found that V_{CA} in $CD4^+$ T cells and macrophages as well as V_{CF} are mainly localized in T-cell zones at and before 10 dpi, in contrast, at 14 and 28 dpi , vRNA loads mainly shifted to B-cell follicles that were associated with FDC networks in the viral form of V_{FDC} and to a less degree as the viral form of V_{CA} in CD4 T cells and Macrophages. The B-cell follicles in LTs are anatomically and functionally unique, as there is a low frequency of CD8 T cells and a high abundance of infectious V_{FDC}, thus B-cell follicles may be more favorable niche for viruses to survival through evading host's immune attack and uninfected CD4 T cell and macrophages get infected by V_{FDC}.

In summary, using the RMs-SIV rectal transmission model, highly sensitive RNAscope and Comb-CODEX-RNAscope, we unambiguously demonstrated that SIV rectal transmission is not a staged disseminate model and viral local replication and amplification is not a precondition for the establishment of systemic infection, and an effective HIV vaccine needs to provide robust protection not only at the portal of virus entry but at the systemic level.

ACKNOWLEDGMENTS

This work was supported by the National Institutes of Health, R01 DK087625, P51OD010425, R24OD011157, and R24OD011172.

Reference:

1. Davis BM, Rall GF, Schnell MJ. 2015. Everything You Always Wanted to Know About Rabies Virus (But Were Afraid to Ask). Annu Rev Virol 2:451-71.

361 2. Murphy FA, Bauer SP, Harrison AK, Winn WC, Jr. 1973. Comparative pathogenesis of rabies and
362 rabies-like viruses. Viral infection and transit from inoculation site to the central nervous system.
363 Lab Invest 28:361-76.
364 3. Racaniello VR. 2006. One hundred years of poliovirus pathogenesis. Virology 344:9-16.
365 4. Beyrer C, Baral SD, Van Griensven F, Goodreau SM, Chariyalertsak S, Wirtz AL, Brookmeyer R.
366 2012. Global epidemiology of HIV infection in men who have sex with men. The Lancet 380:367-
367 377.
368 5. Ribeiro Dos Santos P, Rancez M, Pretet JL, Michel-Salzat A, Messent V, Bogdanova A, Couedel-
369 Courteille A, Souil E, Cheynier R, Butor C. 2011. Rapid dissemination of SIV follows multisite
370 entry after rectal inoculation. PLoS One 6:e19493.
371 6. Yongjun Sui EML, Yichuan Wang, Alison Hogg, Blake Frey, David Venzon, Ranajit Pal, and Jay A.
372 Berzofsky. 2016. Early SIV Dissemination After Intrarectal SIVmac251 Challenge Was Associated
373 With Proliferating Virus-Susceptible Cells in the Colorectum. J Acquir Immune Defic Syndr
374 71:353–358.
375 7. Kelley CF, Kraft CS, de Man TJ, Duphare C, Lee HW, Yang J, Easley KA, Tharp GK, Mulligan MJ,
376 Sullivan PS, Bosinger SE, Amara RR. 2017. The rectal mucosa and condomless receptive anal
377 intercourse in HIV-negative MSM: implications for HIV transmission and prevention. Mucosal
378 Immunol 10:996-1007.
379 8. Deleage C, Immonen TT, Fennessey CM, Reynaldi A, Reid C, Newman L, Lipkey L, Schlub TE,
380 Camus C, O'Brien S, Smedley J, Conway JM, Del Prete GQ, Davenport MP, Lifson JD, Estes JD,
381 Keele BF. 2019. Defining early SIV replication and dissemination dynamics following vaginal
382 transmission. Sci Adv 5:eaav7116.
383 9. Deleage C, Wietgrefe SW, Del Prete G, Morcock DR, Hao XP, Piatak M, Jr., Bess J, Anderson JL,
384 Perkey KE, Reilly C, McCune JM, Haase AT, Lifson JD, Schacker TW, Estes JD. 2016. Defining HIV
385 and SIV Reservoirs in Lymphoid Tissues. Pathog Immun 1:68-106.
386 10. Haase AT. 2011. Early events in sexual transmission of HIV and SIV and opportunities for
387 interventions. Annu Rev Med 62:127-39.
388 11. Martins MA, Gonzalez-Nieto L, Ricciardi MJ, Bailey VK, Dang CM, Bischof GF, Pedreño-Lopez N,
389 Pauthner MG, Burton DR, Parks CL, Earl P, Moss B, Rakasz EG, Lifson JD, Desrosiers RC, Watkins DI.
390 2020. Rectal Acquisition of Simian Immunodeficiency Virus (SIV) SIVmac239 Infection despite
391 Vaccine-Induced Immune Responses against the Entire SIV Proteome. J Virol 94.
392 12. Brandon F. Keele FVH, Yingying Li, Elizabeth Bailes, Jun Takehisa, Mario L. Santiago, Frederic
393 Bibollet-Ruche, Yalu Chen, Louise V. Wain, Severin Loul, Eitel Mpoudi Ngole, Yanga Bienvenue,
394 Eric Delaporte, John F. Y. Brookfield, Paul M. Sharp, George M. Shaw, Martine Peeters, Beatrice H.
395 Hahn. 2006. Chimpanzee reservoirs of pandemic and nonpandemic HIV-1. Science.
396 13. Smyth RP, Davenport MP, Mak J. 2012. The origin of genetic diversity in HIV-1. Virus Res 169:415-
397 29.
398 14. Whitney JB, Lim SY, Osuna CE, Kublin JL, Chen E, Yoon G, Liu PT, Abbink P, Borducci EN, Hill A,
399 Lewis MG, Geleziunas R, Robb ML, Michael NL, Barouch DH. 2018. Prevention of SIVmac251
400 reservoir seeding in rhesus monkeys by early antiretroviral therapy. Nat Commun 9:5429.
401 15. Shaw GM, Hunter E. 2012. HIV transmission. Cold Spring Harb Perspect Med 2.
402 16. Yu M, Vajdy M. 2010. Mucosal HIV transmission and vaccination strategies through oral
403 compared with vaginal and rectal routes. Expert Opin Biol Ther 10:1181-95.
404 17. Evans DT, Silvestri G. 2013. Nonhuman primate models in AIDS research. Curr Opin HIV AIDS
405 8:255-61.
406 18. García-Lerma JG, Heneine W. 2012. Animal models of antiretroviral prophylaxis for HIV
407 prevention. Current Opinion in HIV and AIDS 7:505-513.

408 19. Lu W, Ma F, Churbanov A, Wan Y, Li Y, Kang G, Yuan Z, Wang D, Zhang C, Xu J, Lewis M, Li Q. 2014.
409 Virus-host mucosal interactions during early SIV rectal transmission. Virology 464-465:406-414.
410 20. Demers A, Kang G, Ma F, Lu W, Yuan Z, Li Y, Lewis M, Kraiselburd EN, Montaner L, Li Q. 2014. The
411 mucosal expression pattern of interferon-ε in rhesus macaques. J Leukoc Biol 96:1101-7.
412 21. Anne Coue¨del-Courteille, Nathalie Barget SbJ, a Jean-Ge´rard Guillet,, Alain Venet c, and Ce´cile
413 Butor. 2003. Delayed viral replication and CD4+ T cell depletion in the rectosigmoid mucosa of
414 macaques during primary rectal SIV infection. Virology 316:290-301.
415 22. Maric D, Corbin L, Greco N, Lorenzo-Redondo R, McRaven MD, Veazey RS, Hope TJ. 2023.
416 Temporal and spatial characterization of HIV/SIV infection at anorectal mucosa using rhesus
417 macaque rectal challenge model. bioRxiv doi:10.1101/2023.02.22.529624.
418 23. Lu W, Demers AJ, Ma F, Kang G, Yuan Z, Wan Y, Li Y, Xu J, Lewis M, Li Q. 2015. Next-Generation
419 mRNA Sequencing Reveals Pyroptosis-Induced CD4+ T Cell Death in Early Simian
420 Immunodeficiency Virus-Infected Lymphoid Tissues. J Virol 90:1080-7.
421 24. Yuan Z, Wang N, Kang G, Niu W, Li Q, Guo J. 2017. Controlling Multicycle Replication of Live-
422 Attenuated HIV-1 Using an Unnatural Genetic Switch. ACS Synth Biol 6:721-731.
423 25. Ko A, Kang G, Hattler JB, Galadima HI, Zhang J, Li Q, Kim WK. 2019. Macrophages but not
424 Astrocytes Harbor HIV DNA in the Brains of HIV-1-Infected Aviremic Individuals on Suppressive
425 Antiretroviral Therapy. J Neuroimmune Pharmacol 14:110-119.
426 26. Cheng Y, Burrack RK, Li Q. 2022. Spatially Resolved and Highly Multiplexed Protein and RNA In
427 Situ Detection by Combining CODEX With RNAscope In Situ Hybridization. J Histochem Cytochem
428 70:571-581.
429 27. Rangaprakash D, Odemuyiwa T, Narayana Dutt D, Deshpande G. 2020. Density-based clustering
430 of static and dynamic functional MRI connectivity features obtained from subjects with cognitive
431 impairment. Brain Inform 7:19.
432 28. Jiang X, Dudzinski S, Beckermann KE, Young K, McKinley E, McIntyre JO, Rathmell JC, Xu J, Gore JC.
433 2020. MRI of tumor T cell infiltration in response to checkpoint inhibitor therapy. Journal for
434 ImmunoTherapy of Cancer 8:e000328.
435 29. Heesters BA, Lindqvist M, Vagefi PA, Scully EP, Schildberg FA, Altfeld M, Walker BD, Kaufmann DE,
436 Carroll MC. 2015. Follicular Dendritic Cells Retain Infectious HIV in Cycling Endosomes. PLoS
437 Pathog 11:e1005285.
438 30. Wang X, Vincent E, Siddiqui S, Turnbull K, Lu H, Blair R, Wu X, Watkins M, Ziani W, Shao J, Doyle-
439 Meyers LA, Russell-Lodrigue KE, Bohm RP, Veazey RS, Xu H. 2022. Early treatment regimens
440 achieve sustained virologic remission in infant macaques infected with SIV at birth. Nature
441 Communications 13:4823.
442 31. Igarashi T, Endo Y, Nishimura Y, Buckler C, Sadjadpour R, Donau OK, Dumaurier MJ, Plishka RJ,
443 Buckler-White A, Martin MA. 2003. Early control of highly pathogenic simian immunodeficiency
444 virus/human immunodeficiency virus chimeric virus infections in rhesus monkeys usually results
445 in long-lasting asymptomatic clinical outcomes. J Virol 77:10829-40.
446 32. Haase AT. 2010. Targeting early infection to prevent HIV-1 mucosal transmission. Nature
447 464:217-23.
448 33. Staprans SI, Dailey PJ, Rosenthal A, Horton C, Grant RM, Lerche N, Feinberg MB. 1999. Simian
449 immunodeficiency virus disease course is predicted by the extent of virus replication during
450 primary infection. J Virol 73:4829-39.
451 34. Veazey RS, Gauduin M-C, Mansfield KG, Tham IC, Altman JD, Lifson JD, Lackner AA, Johnson RP.
452 2001. Emergence and Kinetics of Simian Immunodeficiency Virus-Specific $CD8^+$ T Cells in the
453 Intestines of Macaques during Primary Infection. 75:10515-10519.
454 35. Deleage C, Immonen TT, Fennessey CM, Reynaldi A, Reid C, Newman L, Lipkey L, Schlub TE,
455 Camus C, O'Brien S, Smedley J, Conway JM, Del Prete GQ, Davenport MP, Lifson JD, Estes JD,

456 Keele BF. 2019. Defining early SIV replication and dissemination dynamics following vaginal
457 transmission. 5:eaav7116.
458 36. Abel K, Pahar B, Van Rompay KK, Fritts L, Sin C, Schmidt K, Colón R, McChesney M, Marthas ML.
459 2006. Rapid virus dissemination in infant macaques after oral simian immunodeficiency virus
460 exposure in the presence of local innate immune responses. J Virol 80:6357-67.
461 37. Milush JM, Chen H-L, Atteberry G, Sodora D. 2013. Early Detection of Simian Immunodeficiency
462 Virus in the Central Nervous System Following Oral Administration to Rhesus Macaques. Volume
463 4 - 2013.
464 38. Deleage C, Chan CN, Busman-Sahay K, Estes JD. 2018. Next-generation in situ hybridization
465 approaches to define and quantify HIV and SIV reservoirs in tissue microenvironments.
466 Retrovirology 15:4.
467 39. Jiang S, Chan CN, Rovira-Clavé X, Chen H, Bai Y, Zhu B, McCaffrey E, Greenwald NF, Liu C, Barlow
468 GL, Weirather JL, Oliveria JP, Nakayama T, Lee IT, Matter MS, Carlisle AE, Philips D, Vazquez G,
469 Mukherjee N, Busman-Sahay K, Nekorchuk M, Terry M, Younger S, Bosse M, Demeter J, Rodig SJ,
470 Tzankov A, Goltsev Y, McIlwain DR, Angelo M, Estes JD, Nolan GP. 2022. Combined protein and
471 nucleic acid imaging reveals virus-dependent B cell and macrophage immunosuppression of
472 tissue microenvironments. Immunity 55:1118-1134.e8.
473 40. Moysi E, Del Rio Estrada PM, Torres-Ruiz F, Reyes-Terán G, Koup RA, Petrovas C. 2021. In Situ
474 Characterization of Human Lymphoid Tissue Immune Cells by Multispectral Confocal Imaging
475 and Quantitative Image Analysis; Implications for HIV Reservoir Characterization. Volume 12 -
476 2021.
477 41. Raehtz KD, Xu C, Deleage C, Ma D, Policicchio BB, Brocca-Cofano E, Piccolo D, Weaver K, Keele BF,
478 Estes JD, Apetrei C, Pandrea I. 2024. Rapid systemic spread and minimal immune responses
479 following SIVsab intrarectal transmission in African green monkeys. JCI Insight 9.
480 42. Ribeiro dos Santos P, Rancez M, Prétet J-L, Michel-Salzat A, Messent V, Bogdanova A, Couëdel-
481 Courteille A, Souil E, Cheynier R, Butor C. 2011. Rapid Dissemination of SIV Follows Multisite
482 Entry after Rectal Inoculation. PLOS ONE 6:e19493.
483 43. Allers K, Kunkel D, Hofmann J, Stahl-Hennig C, Moos V, Schneider T. 2018. Cell-Associated Simian
484 Immunodeficiency Virus Accelerates Initial Virus Spread and CD4+ T-Cell Depletion in the
485 Intestinal Mucosa. The Journal of Infectious Diseases 217:1421-1425.

486

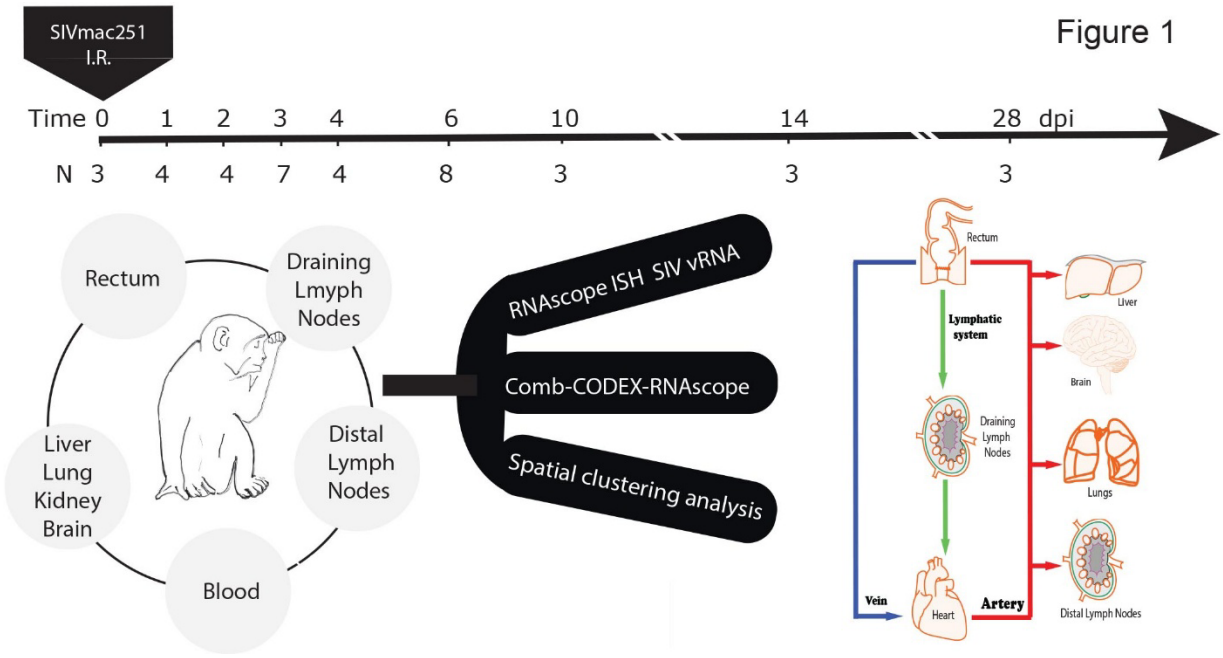

Figure 1. Experimental Design and Euthanasia Timeline of Rhesus Macaques Following Rectal SIVmac251 Inoculation.

Upper panel shows the timeline for animal euthanasia following SIV rectal inoculation with animal numbers per time point. Lower panel shows the sampling strategy and assays utilized to track viral spatiotemporal distribution patterns across macaque organ systems.

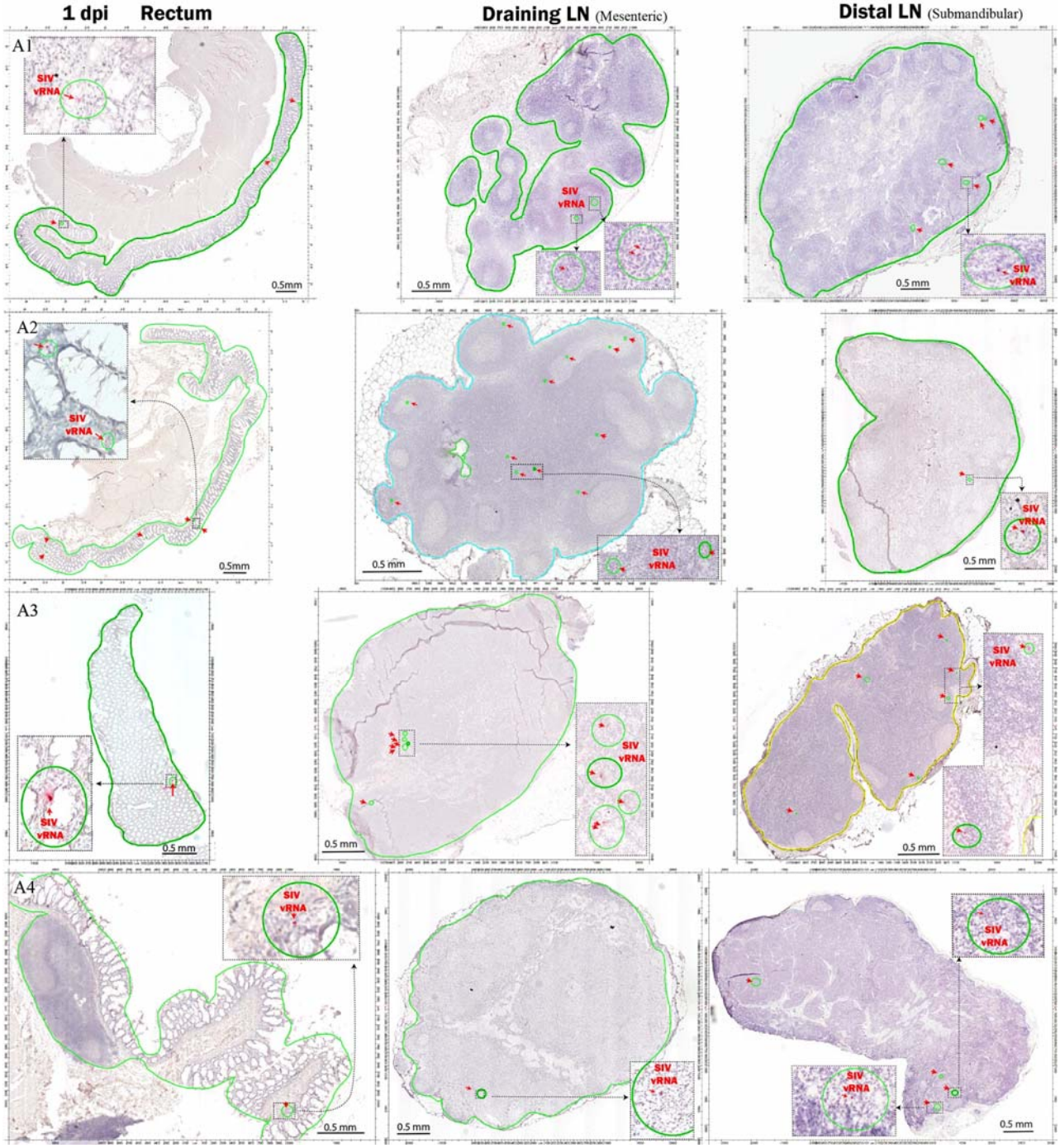
1 dpi
Rectum
Draining LN (Mesenteric)
Distal LN (Submandibular)
A1
A2
A3
A4
SIV vRNA
0.5mm
0.5 mm

Figure 2. SIV viral RNA (vRNA) was detected in rectum draining lymph node (dLN) and distal lymph node (disLN) tissues obtained from four macaques on day 1 post SIV inoculation.

Representative micrographs showing SIV vRNA in rectal tissue, dLN (mesenteric), and disLN (mandibular) from all four rhesus macaques at 1 dpi. The vRNA was visualized as distinct red punctate signals with SIVmac239 antisense probes and Fast Red chromogen and cell nuclei were counterstained blue using hematoxylin. Rows designated as A1-4, each represents an individual macaque, and columns show the rectum, dLN and disLN tissues, respectively. Red arrow and green circle highlight vRNA signals. Higher magnification insets from the boxed regions of each tissue section are displayed.

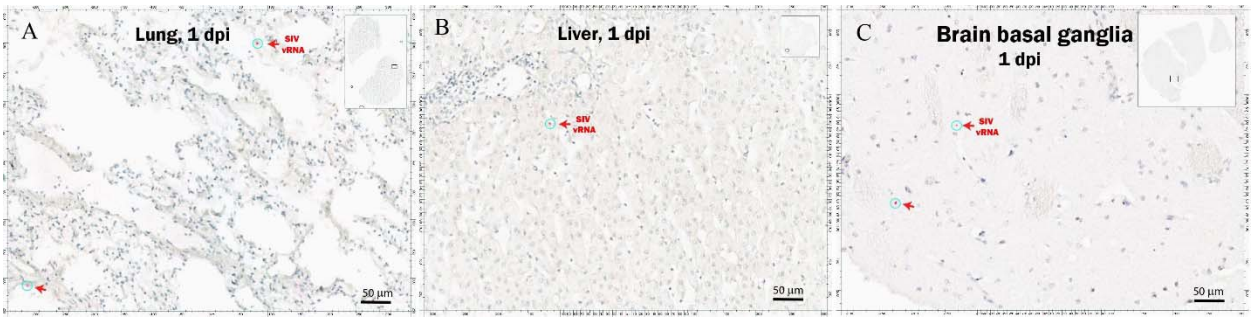

Figure 3. SIV vRNA was detectable in non-lymphoid organs of lungs, liver and brain tissues obtained from four macaques on day 1 post SIV inoculation.

Representative micrographs from a small boxed area of insets showing SIV vRNA in lung (**A**), liver (**B**), and brain basal ganglia (**C**) of a macaque A1 at 1 dpi. The vRNA was visualized as distinct red punctate signals with SIVmac239 antisense probes and Fast Red chromogen and cell nuclei were counterstained blue using hematoxylin. Red arrows and green circles highlight vRNA signals.

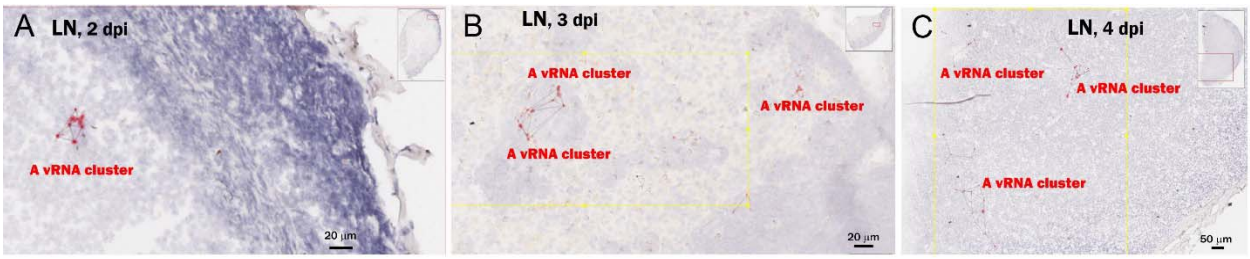

Figure 4. SIV vRNA clusters present in lymph node tissues on 2, 3, and 4 dpi, but not 1 dpi.

Representative micrographs from a small boxed area of insets show SIV vRNA clusters within draining lymph node (dLN) tissues collected from macaques at 2, 3, and 4 dpi. vRNA clusters were identified through implementation of the Density-Based Spatial Clustering of Applications with Noise (DBSCAN) algorithm within QuPath image analysis software. A vRNA cluster is defined as ≥3 individual vRNA signals within 50 µm diameter regions. vRNA was detected using RNAscope. (A) shows 2 dpi, (B) 3 dpi, and (C) 4 dpi. No viral clustering was observed at 1 day post-infection across rectal tissue, draining lymph nodes, or distal lymph node specimens. Higher magnification insets from the boxed regions of each tissue section are displayed. Red arrows and green circles highlight vRNA signals.

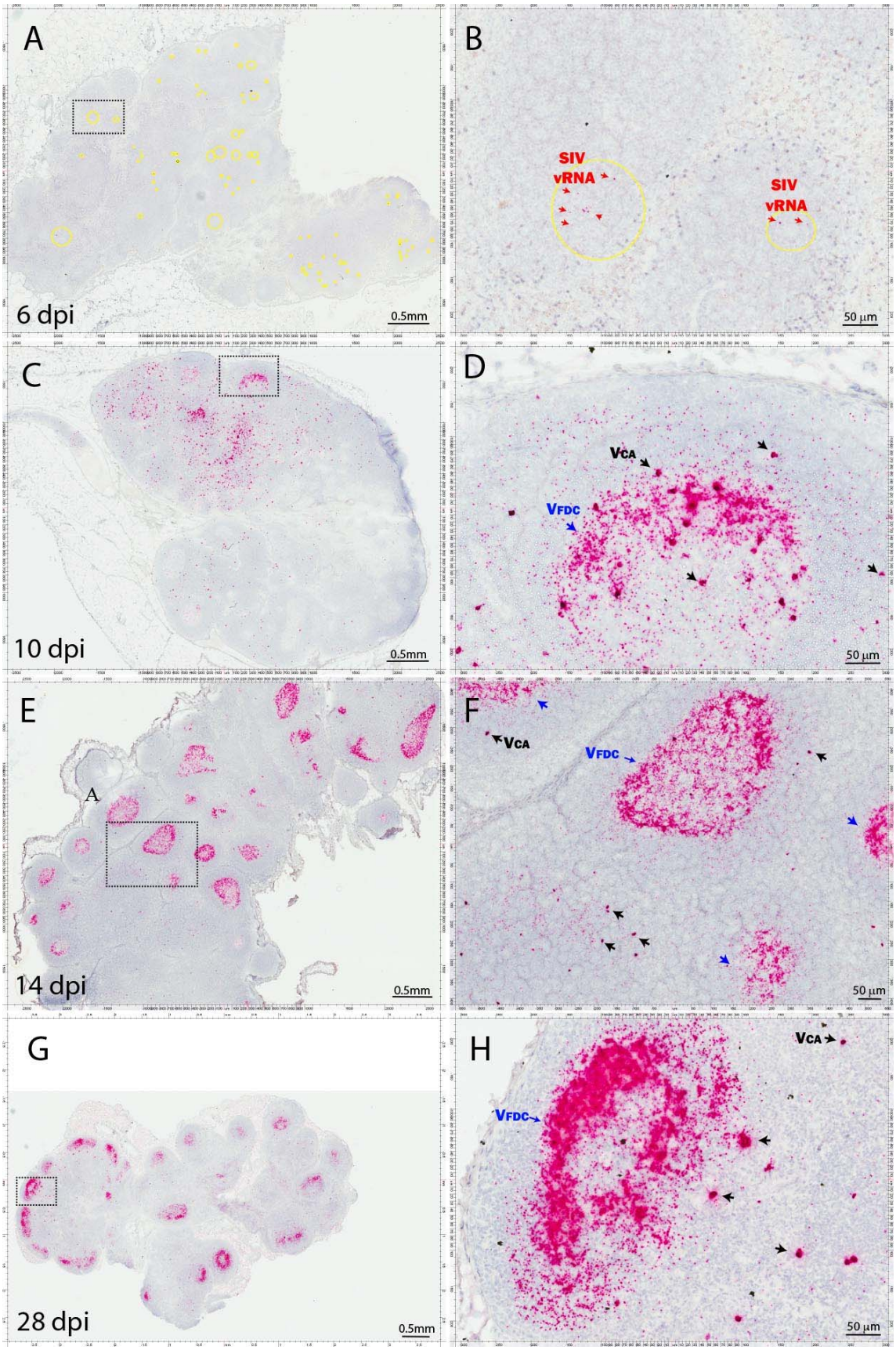
A
6 dpi
0.5mm
B
SIV
vRNA
SIV
vRNA
50 µm
C
10 dpi
0.5mm
D
VCA
VFDC
50 µm
E
A
14 dpi
0.5mm
F
VCA
VFDC
50 µm
G
28 dpi
0.5mm
H
VCA
VFDC
50 µm

Figure 5. Temporal and spatial dynamics of three distinct viral forms in lymph node tissues during acute SIV rectal infection

Representative micrographs show three distinct viral forms, e.g., cell-free viruses (Vcf), cell-associated viruses (Vca), and follicular dendritic cell-trapped viruses (VFDC) in LN tissues during early rectal infection. At 6 dpi (panels A and B), vRNA was exclusively detected as Vca and Vcf populations, with Vcf appearing as discrete signals external to cellular boundaries. By 10 dpi (panels C and D), VFDC first became detectable, characterized by diffuse vRNA signal patterns in the B follicles. The VFDC population emerged as the predominant viral form at both 14 dpi (panels E and F) and 28 dpi (panels G and H). Higher magnification images on the right side of each panel provide detailed visualization of the boxed regions from the corresponding left-side overview images.

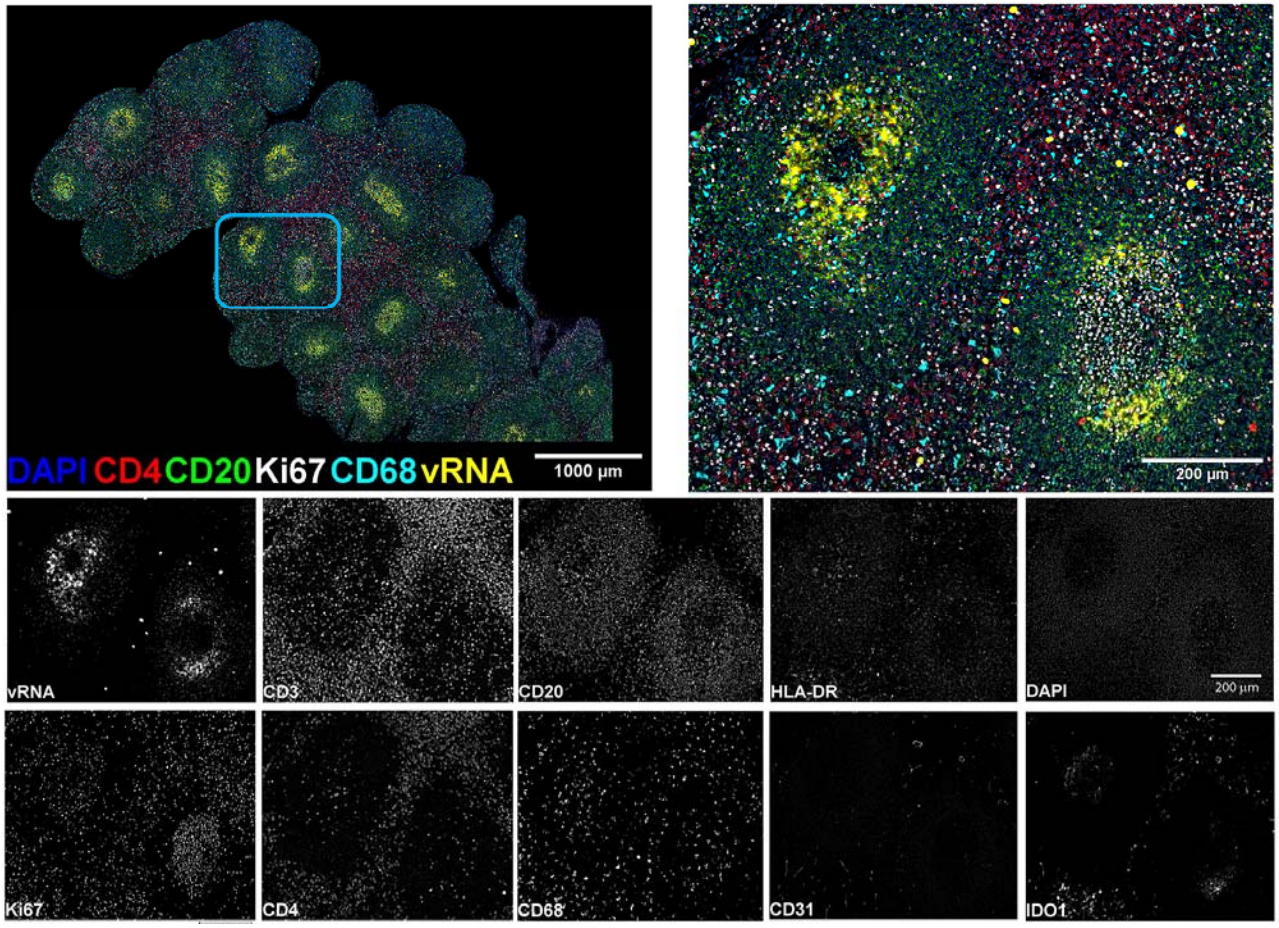

Figure 6. Representative Comb-CODEX-RNAscope imaging of lymph node tissues.

The upper-left image displays the complete lymph node cross-section (28 dpi, Rh5429) with overlay of some fluorescent signal channels, with respective markers and corresponding color assignments as indicated. **The lower smaller panels** display magnified views of the designated boxed regions from the overview image, with each image showing individual detection channels. The **upper-right image shows a**n additional magnified view of the designated boxed regions from the overview image.

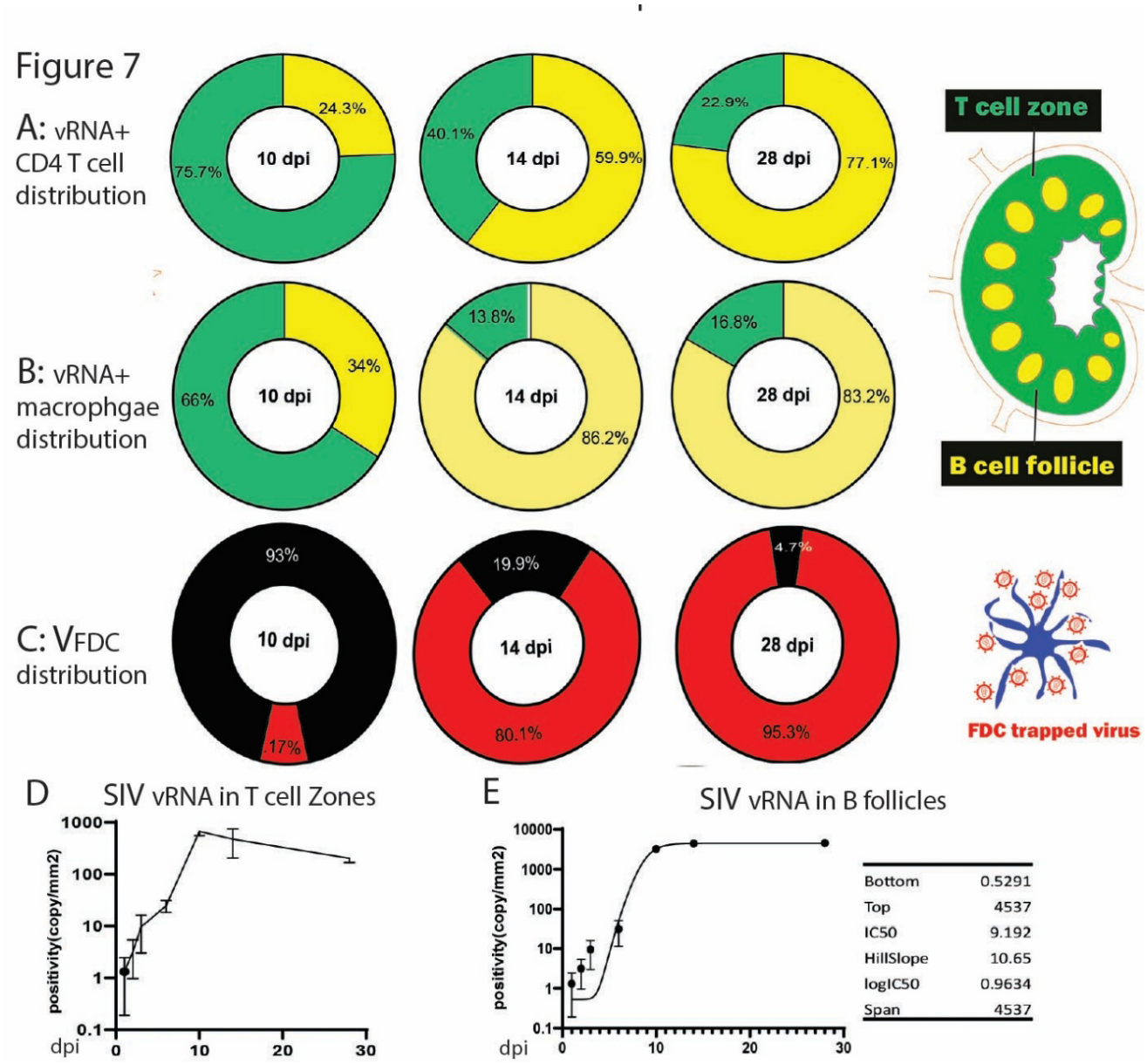

Fig 7 The spatiotemporal distribution patterns of virally infected cells in lymphatic tissues during early rectal transmission

SIV vRNA was detected using Comb-CODEX-RNAscope and the spatial distribution patterns of vRNA+ cells in T-cell zones versus B-cell follicles of mesenteric LN tissues over time were quantified CODEX processor software. The percentage of SIV vRNA+ CD4 T cells (**A)**, vRNA+ macrophages (**B)** in T-cell zones versus B-cell follicles as well as the percentage of follicular

dendritic cell–associated virions (VFDC) in total vRNA signals over time of 10, 14 and 28 dpi (n=3/each time) . (**C**) SIV vRNA in vivo viral growth curves in T-cell zones (**D**) and in B-cell follicles, include Vca and VFDC (**E**) throughout early rectal transmission (n=4 at 1, 2, 3 dpi and n=3 at 6, 10, 14, 28 dpi).

Supplemental Table 1

SIV vRNA Detection and Quantification in Brain, Liver and Lung Tissues During Early Rectal Transmission Using RNAscope In Situ Hybricyzation

ID	vRNA	Frontal Cortex				Basal Ganglia				Liver				Lung			
		vRNA	Area	Pos #	#/mm2	vRNA	Area	Pos #	#/mm2	vRNA	Area	Pos #	#/mm2	vRNA	Area	Pos #	#/mm2
A1	1	+	2.7	1	0.37	+	21.5	21	0.98	+	37.2	2	0.05	+	45.7	88	1.93
A2	1	+	28.9	38	1.32	+	14.8	8	0.53	+	41.7	2	0.05	+	26.9	43	1.6
A3	1	+	49.6	67	1.35	+	29.7	30	1.01	+	24.5	2	0.08	+	35.0	40	1.14
A4	1	+	12.9	4	0.31	+	30.8	23	0.75	+	15.8	1	0.06	+	14.4	46	3.21
B1	2	+	9.0	12	1.34	+	13.8	20	1.45	+	17.6	12	0.68	+	18.3	14	0.77
B2	2	+	36.9	7	0.19	+	7.7	27	3.53	+	56.3	9	0.16	+	15.6	33	2.12
B3	2	+	53.3	34	0.64	+	93.1	45	0.48	+	37.7	15	0.4	+	30.1	49	1.63
B4	2	+	33.8	5	0.15	+	73.1	50	0.68	+	47.8	4	0.08	+	19.9	38	1.91
C1	3	+	18.8	26	1.38	+	33.6	111	3.31	+	62.6	13	0.21	+	33.3	29	0.87
C2	3	+	52.6	1	0.02	+	62.1	62	1.00	+	52.1	32	0.61	+	14.0	27	1.94
C3	3	+	13.9	5	0.36	+	51.1	53	1.04	+	47.3	8	0.17	+	39.0	23	0.59
C4	3	+	10.8	191	17.7	+	19.3	27	1.40	+	43.3	26	0.6	+	13.8	38	2.76
Rh4971	3	+	103.8	6	0.06	+	119.0	8	0.07	+	97.5	113	1.16	+	101.2	264	2.61
Rh4972	3	+	76.37	13	0.17	+	70.5	1	0.01	+	160.9	3	0.02	+	202.2	108	0.53
Rh4973	3	+	110.7	35	0.32	+	112.5	4	0.04	+	110.2	7	0.06	+	179.8	131	0.73
RhL983	4	+	149.7	10	0.07	+	78.3	1	0.01	+	37.2	108	2.90	+	73.7	128	1.74
Rh5043	4	+	53.6	15	0.28	-	63.9	0	0.00	+	74.6	48	0.64	+	46.3	9	0.19
Rh5044	4	+	35.9	3	0.08	+	56.5	1	0.02	+	36.9	26	0.70	+	37.3	3	0.08
Rh5045	4	+	81.1	18	0.22	+	72.4	10	0.14	+	31.3	30	0.96	+	93.6	28	0.3
RhL864	6	+	32.5	S6	1.72	+	97.3	11	0.11	+	122.5	8	0.07	+	36.5	18	0.49
Rh4809	6	+	97.1	89	0.92	-	128.5	0	0.00	+	31.9	37	1.16	+	S5.2	8	0.15
Rh5052	6	+	89.7	22	0.25	+	39.3	6	0.15	+	43.3	11	0.25	+	45.4	11	0.24
Rh5053	6	+	70.6	9	0.13	+	27.4	3	0.11	+	85.3	35	0.41	+	53.7	71	1.32
D1	6	+	61.3	3	0.05	+	124.3	37	0.30	+	42.3	75	1.77	+	63.5	21	0.33
D2	6	+	12.3	6	0.49	+	43.9	16	0.36	+	65.3	2	0.03	+	14.8	5	0.34
D3	6	+	12.37	1	0.08	+	17.2	10	0.58	+	23.7	40	1.69	+	26.1	7	0.27
D4	6	+	3.29	18	5.47	+	27.7	12	0.43	+	36.0	15	0.42	+	12.3	7	0.57

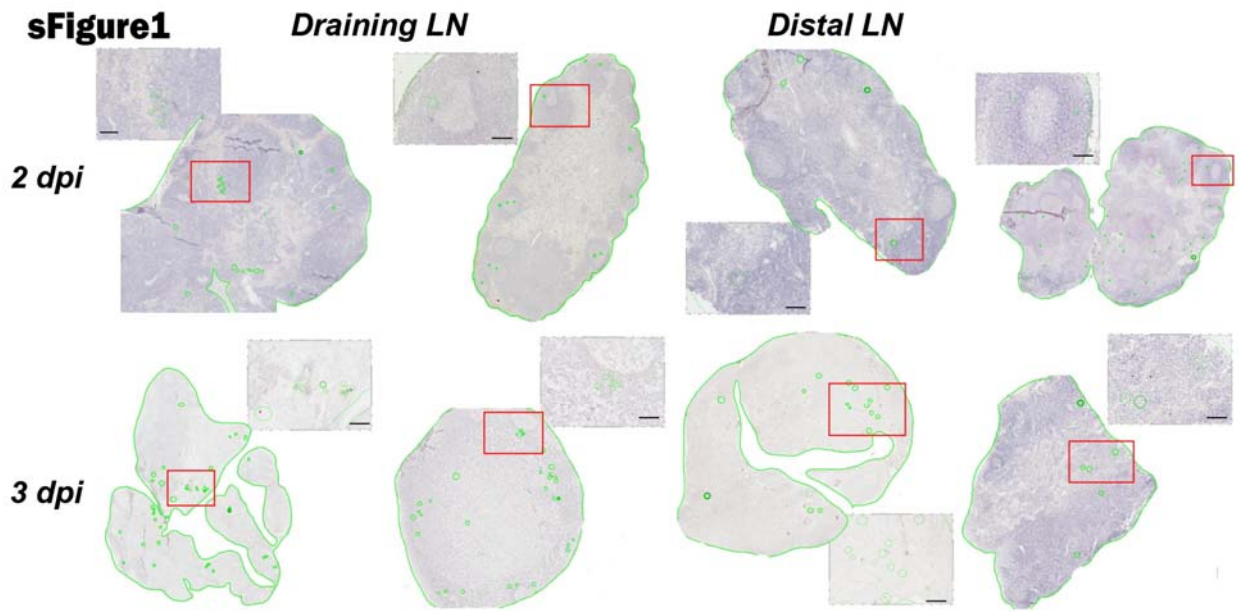

Supplemental Figure1. SIV viral RNA (vRNA) in the draining lymph node (dLN) and distal lymph node (disLN) tissues on 2 and 3 dpi.

Representative micrographs showing SIV vRNA in dLN (mesenteric), and disLN (mandibular) from all 2 rhesus macaques at 2 dpi (B1 & B4) and 3 dpi (C1 &C2). The vRNA was visualized as distinct red punctate signals with SIVmac239 antisense probes and Fast Red chromogen and cell nuclei were counterstained blue using hematoxylin. Green circles highlight vRNA signals. Higher magnification images from the boxed regions of each corresponding tissue section are displayed. Scale bar equals 100 microns.

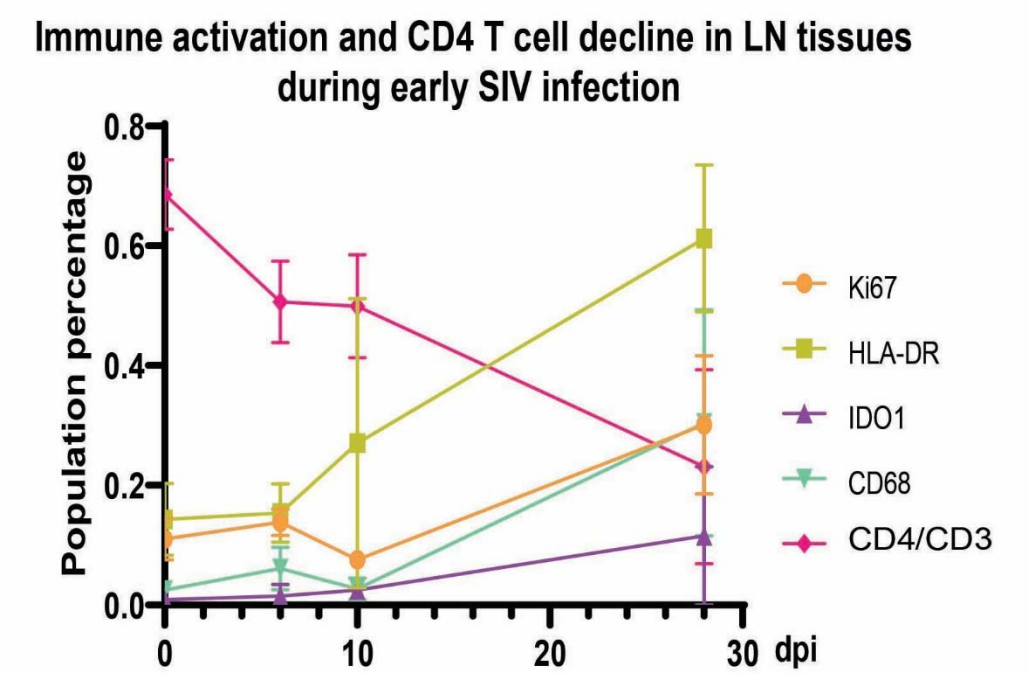

Supplementary Figure 2. Immune activation and CD4 T cell decline in the LN tissues during early SIV rectal infection.

Immune cell markers were detected using Comb-CODEX-RNAscope. CD4 T cells and immune activation markers in the LN tissues of macaques without SIV infection, 6 10 and 28 dpi (n=3/time point) were quantified. There was a significant CD4 T cells decline (CD4/Cd3 ratio), an increased expression of immune activation protein markers of ki67, HLA-Dr as well as immune suppression protein marker of Iindoleamine 2,3-dioxygenase 1 (IDO1).